European Journal of
Mineralogy
Open Access

Crystal chemistry of type paulkerrite and establishment of the paulkerrite group nomenclature

Ian E. Grey[1], **Stephanie Boer**[2], **Colin M. MacRae**[1], **Nicholas C. Wilson**[1], **William G. Mumme**[1], **and Ferdinando Bosi**[3]

[1]CSIRO Mineral Resources, Private Bag 10, Clayton South, Victoria 3169, Australia
[2]Australian Synchrotron, 800 Blackburn Road, Clayton, Victoria 3168, Australia
[3]Department of Earth Sciences, Sapienza University of Rome, Piazzale Aldo Moro 5, 00185 Rome, Italy

Correspondence: Ian E. Grey (ian.grey@csiro.au)

Abstract. A single-crystal structure determination and refinement has been conducted for the type specimen of paulkerrite. The structure analysis showed that the mineral has monoclinic symmetry, space group $P2_1/c$, not orthorhombic, $Pbca$, as originally reported. The unit-cell parameters are $a = 10.569(2)$, $b = 20.590(4)$, $c = 12.413(2)$ Å, and $\beta = 90.33(3)°$. The results from the structure refinement were combined with electron microprobe analyses to establish the empirical structural formula $^{A1}[(H_2O)_{0.98}K_{0.02}]_{\Sigma 1.00}$ $^{A2}K_{1.00}$ $^{M1}(Mg_{1.02}Mn^{2+}_{0.98})_{\Sigma 2.00}$ $^{M2}(Fe^{3+}_{1.20}Ti^{4+}_{0.54}Al_{0.24}Mg_{0.02})_{\Sigma 2.00}$ $^{M3}(Ti^{4+}_{0.74}Fe^{3+}_{0.26})_{\Sigma 1.00}$ $(PO_4)_{4.02}$ $^X[O_{1.21}F_{0.47}(OH)_{0.32}]_{\Sigma 2.00}(H_2O)_{10} \cdot 3.95H_2O$, which leads to the end-member formula $(H_2O)KMg_2Fe_2Ti(PO_4)_4(OF)(H_2O)_{10} \cdot 4H_2O$.

A proposal for a paulkerrite group, comprising orthorhombic members benyacarite, mantiennéite, pleysteinite, and hochleitnerite and monoclinic members paulkerrite and rewitzerite, has been approved by the International Mineralogical Association's Commission for New Minerals, Nomenclature and Classification. The general formulae are $A_2M1_2M2_2M3(PO_4)_4X_2(H_2O)_{10} \cdot 4H_2O$ and $A1A2M1_2M2_2M3(PO_4)_4X_2(H_2O)_{10} \cdot 4H_2O$ for orthorhombic and monoclinic species, respectively, where $A = $ K, H$_2$O, $\square$ ($=$ vacancy); $M1 = $ Mn^{2+}, Mg, Fe^{2+}, Zn (rarely Fe^{3+}); $M2$ and $M3 = $ Fe^{3+}, Al, Ti^{4+} (and very rarely Mg); $X = $ O, OH, F. In monoclinic species, K and H$_2$O show an ordering at the $A1$ and $A2$ sites, whereas O, (OH), and F show a disordering over the two non-equivalent $X1$ and $X2$ sites, which were hence merged as X_2 in the general formula. In both monoclinic and orthorhombic species, a high degree of mixing of Fe^{3+}, Al, and Ti occurs at the $M2$ and $M3$ sites of paulkerrite group members, making it difficult to get unambiguous end-member formulae from the structural determination of the constituents at individual sites. To deal with this problem an approach has been used that involves merging the compositions at the $M2$ and $M3$ sites and applying the site-total-charge method. The merged-site approach allows end-member formulae to be obtained directly from the chemical analysis without the need to conduct crystal-structure refinements to obtain the individual site species.

1 Introduction

The three secondary Ti-bearing phosphate minerals paulkerrite (Peacor et al., 1984), mantiennéite (Fransolet, 1984), and benyacarite (Demartin et al., 1993, 1997) have similar compositions and powder X-ray diffraction patterns, with reported orthorhombic unit-cell parameters $a \sim 10.5$, $b \sim 20.5$, and $c \sim 12.4$ Å. Demartin et al. (1997) gave the general

formula [H$_2$O,K]$_2$Ti$M1_2M2_2$(PO$_4$)$_4$(O,F)$_2 \cdot 14$H$_2$O for the three minerals based on their crystal structure determination for benyacarite (Demartin et al., 1993) in the orthorhombic space group $Pbca$. They noted that the $M1$ site is occupied by divalent cations, with dominant Mn^{2+} in benyacarite and dominant Mg in paulkerrite and mantiennéite, while the $M2$ site has dominant Fe^{3+} in benyacarite and paulkerrite and Al in mantiennéite.

Three minerals closely related to benyacarite have received recent approvals from the International Mineralogical Association (IMA) Commission for New Minerals, Nomenclature and Classification (CNMNC). They are pleysteinite (Grey et al., 2023a) and hochleitnerite (Grey et al., 2023b), isostructural with benyacarite, and rewitzerite (Grey et al., 2023c) with a monoclinic ($P2_1/c$) modification of the *Pbca* benyacarite structure. The six minerals form a group as defined by Mills et al. (2009) with the group name paulkerrite, as the first-described member. The description of paulkerrite however did not include a crystal structure refinement, due to the poor diffracting quality of the crystals (Peacor et al., 1984), raising some doubt about the reported formula. To address this issue, we obtained on loan the type specimen of paulkerrite for crystallographic characterisation and refined the crystal structure using a synchrotron-based single-crystal dataset. The structure analysis showed that type paulkerrite crystals are isostructural with rewitzerite, having monoclinic symmetry, space group $P2_1/c$, a maximum non-isomorphous subgroup of *Pbca*. The study on rewitzerite established a structural formula for monoclinic paulkerrite-group members of $A1A2M1_2M2_2M3(PO_4)_4X_2$ $(H_2O)_{10} \cdot 4H_2O$ (Grey et al., 2023c), where $A1 =$ prevailing K or H_2O, and $A2 =$ prevailing H_2O or K.

A common feature of the monoclinic and orthorhombic crystal structures of paulkerrite-group minerals is a high degree of mixing of Ti, Al, and Fe^{3+} at two non-equivalent but very similar crystallographic sites, $M2$ and $M3$. This makes the assignments of dominant constituents at these two sites (and thus the end-member formulae, as defined by Hawthorne, 2002) very sensitive to the location of minor constituents. This problem can be overcome by merging the compositions of the two sites and then obtaining the correct end-member by the site-total-charge method (Bosi et al., 2019a). Application of this procedure resulted in changes to the end-member formulae for some members of the group. A proposal for the establishment of the paulkerrite group with the application of the site-merging procedure for establishment of end-member formulae as defined by Hawthorne (2002), and the resulting revision of some formulae, has been approved by the IMA CNMNC, proposal revised 22-K-bis. We describe here the crystal-chemical characterisation of type paulkerrite and the establishment and nomenclature of the paulkerrite group.

2 Characterisation of type paulkerrite specimen

2.1 Description of specimen

The type specimen of paulkerrite is from the 7U7 Ranch, about 40 km west of Hillside, Yavapai County, Arizona. We obtained the type specimen on loan from the Smithsonian Institution, Washington, catalogue number NMNH R7778. Its occurrence, associated minerals and physical properties
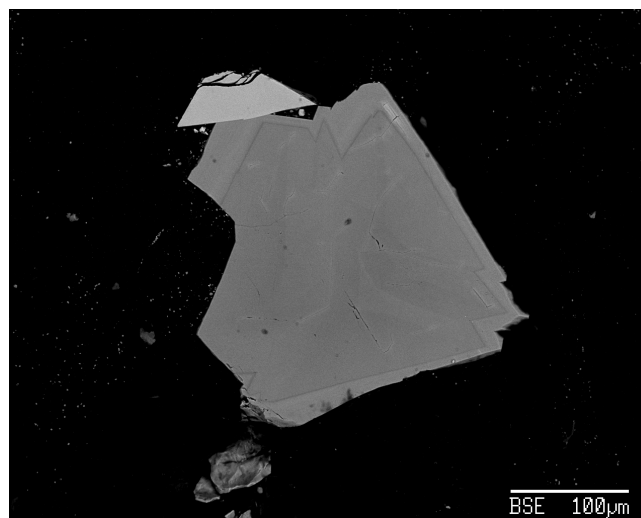
Figure 1. Back-scattered electron image of type paulkerrite showing zoning due to Mg / Mn substitution and a rim of a Mn-rich paulkerrite-group mineral. Bright sliver of triplite at top of crystal.

are described by Peacor et al. (1984). Isolated tabular light-brown crystals of paulkerrite are dispersed with bermanite on fracture surfaces on triplite. Hurlbut (1936), who first reported paulkerrite at the Arizona pegmatite as an unidentified phosphate mineral, gave an analysis of triplite corresponding to $MnMg_{0.65}Fe_{0.35}(PO_4)F$. It is likely that the Mg-bearing triplite is the precursor mineral for paulkerrite, with K, Al, and Ti being provided by decomposed muscovite in the pegmatite surrounding the triplite segregation. Peacor et al. (1984) presented electron microprobe analyses for paulkerrite and noted that the Fe was predominantly Fe^{3+} based on microchemical tests. They assigned the oxidation state of Mn as Mn^{2+} based on a better match to the optical properties than for Mn^{3+}. They did note, however, that the triplite matrix mineral is frequently black in colour due to Mn oxidation, and the closely associated mineral bermanite is a mixed Mn valence mineral, $Mn^{2+}Mn_2^{3+}(PO_4)_2(OH)_2 \cdot 4H_2O$.

2.2 Chemical analysis

Tabular crystals of paulkerrite similar to those shown in Figs. 1 to 3 of Peacor et al. (1984) were prepared in a polished epoxy mount for scanning electron microscopy (SEM) and electron microprobe (EMP) analyses. The crystals showed complex chemical zoning due to variations in Mg versus Mn. A back-scattered electron (BSE) image showing the zoning is shown in Fig. 1. In addition, the crystals all displayed a rim, typically 5 to 10 μm wide, enriched in Mn, that has a lighter colour in the BSE image of Fig. 1.

Crystals of type paulkerrite were analysed using wavelength-dispersive spectrometry on a JEOL JXA-8500F Hyperprobe operated at an accelerating voltage of 15 kV and a beam current of 2.2 nA. The beam was defocused to 10 μm
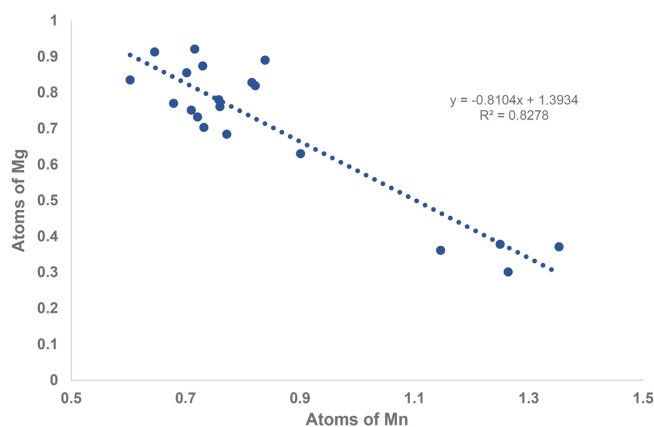
Figure 2. Plot of atoms of Mn versus atoms of Mg from EMP analysis of paulkerrite crystals.

(5 μm for rim analyses). Analytical EMP results are given in Table 1 for analyses made in the core regions of crystals (16 analyses) and in the rims (3 analyses). The analyses of Peacor et al. (1984) are included for comparison. There was insufficient material for direct determination of H_2O, so it was based upon the crystal structure analysis with 15 H_2O per 4 PO_4. The water content was used in the matrix correction of the raw EMP data. Bond valence sums (BVSs) calculated from refined bond distances using the parameters of Gagné and Hawthorne (2015) confirmed that the Fe was in the trivalent state only. The mean wt % oxides for the core analyses agree with the analyses reported by Peacor et al. (1984) to within 1–2 SDs. The atomic fractions, scaled to $5M$ cations and 33 anions, are as follows:

core : $K_{1.02}Mg_{1.04}Mn_{0.98}Fe^{3+}_{1.47}Al_{0.24}Ti_{1.27}P_{4.02}F_{0.47}O_{32.53}H_{30.16}$

rim : $K_{1.00}Mg_{0.43}Mn_{1.57}Fe^{3+}_{1.82}Al_{0.03}Ti_{1.15}P_{3.93}F_{0.63}O_{31.82}H_{29.48}$.

A comparison of the two formulae shows that the major chemical change from the core to the rim is substitution of Mg by Mn. This change is illustrated by the strong negative correlation shown in the scatter plot in Fig. 2. A weaker negative correlation is associated with Fe replacing Al and Ti in the rim, with an increase in the F content.

To express the atomic fractions in the crystal core as a structure-based empirical formula, the least-squares program OccQP (Wright et al., 2000) was used to optimise the site occupations for the $M1$ to $M3$ sites, which were then combined with the EMP analyses for K and F: $^{A1}[(H_2O)_{0.98}K_{0.02}]_{\Sigma1.00}$ $^{A2}K_{1.00}$ $^{M1}(Mg_{1.02}Mn^{2+}_{0.98})_{\Sigma2.00}$ $^{M2}(Fe^{3+}_{1.20}Ti^{4+}_{0.54}Al_{0.24}Mg_{0.02})_{\Sigma2.00}$ $^{M3}(Ti^{4+}_{0.74}Fe^{3+}_{0.26})_{\Sigma1.00}$ $(PO_4)_{4.02}$ $^X[O_{1.21}F_{0.47}(OH)_{0.32}]_{\Sigma2.00}$ $(H_2O)_{10} \cdot 3.95H_2O$.

Note that the two X sites are non-equivalent ($X1$ and $X2$) in the monoclinic symmetry, but as O, (OH), and F are disordered over them, they were merged as X_2. By contrast, K and H_2O show an ordering at two non-equivalent $A1$ and $A2$ sites. The above formula has dominant Mg at

$M1$, Fe^{3+} at $M2$, and Ti at $M3$, consistent with the reported site occupations for paulkerrite (Peacor et al., 1984; Demartin et al., 1997) and giving the end-member formula $(H_2O)KMg_2Fe_2Ti(PO_4)_4(OF)(H_2O)_{10} \cdot 4H_2O$.

Single-crystal diffraction data could not be obtained on the thin, Mn-rich rims of the paulkerrite crystals, so the procedure used for the crystal cores could not be used to determine the end-member formula. Instead, the merged-site procedure, described in Sect. 3.2, was applied. In this approach, the larger divalent cations from the EMP analyses are assigned to the $M1$ site, and the remaining smaller cations are assigned to the $(M2 + M3)$ sites. These are combined with the K and F from EMP analyses to obtain the empirical formula of the rim zones: $^{A1}(H_2O)_{1.00}$ $^{A2}K_{1.00}$ $^{M1}(Mn_{1.57}Mg_{0.43})_{\Sigma2.00}$ $^{M2+M3}(Fe^{3+}_{1.82}Ti_{1.15}Al_{0.03})_{\Sigma2.00}(PO_4)_{3.93}$ $^X(F_{0.63}(OH)_{0.01}$ $O_{1.36})_{\Sigma2.00}(H_2O)_{10} \cdot 3.74H_2O$.

The composition at the $(M2_2M3)$ merged sites is dominated by the atomic arrangement (Fe₂Ti), as will be described in Sect. 3.2. The resulting end-member formula corresponding to the crystal rims is $(H_2O)KMn_2Fe_2Ti(PO_4)_4(OF)(H_2O)_{10} \cdot 4H_2O$. This is the same as the end-member formula for the crystal cores, except for the replacement of Mg by Mn as the dominant $M1$ site constituent.

2.3 Crystallography

Single-crystal diffraction data were collected on a crystal of type paulkerrite at the Australian Synchrotron MX2 microfocus beamline (Aragao et al., 2018). Intensity data were collected using a Dectris EIGER 16M detector and monochromatic radiation with a wavelength of 0.7109 Å. The crystal was maintained at 100 K in an open-flow nitrogen cryostream during data collection. The diffraction data were collected using a single 21 s sweep of 360° rotation around ϕ. The resulting dataset consists of 3600 individual images with an approximate ϕ angle of each image being 0.1°. The raw intensity dataset was processed using XDS software to produce data files that were analysed using WinGX (Farrugia, 1999) and Jana2006 (Petříček et al., 2014).

A structural model was obtained in monoclinic space group $P2_1/c$ using SHELXT (Sheldrick, 2015) and found to be closely related to the orthorhombic, $Pbca$ structures for benyacarite and pleysteinite. In the monoclinic space group the cation sites in the $Pbca$ structures are each split into pairs of sites, $A1 / A2$, $M1a / M1b$, $M2a / M2b$, and $M3a / M3b$, at positions x, y, z and $1/2 + x$, $1/2 - y$, $-z$. The same atom labelling was used as for the orthorhombic minerals, for ease of comparison. Based on previous structural studies of paulkerrite-group minerals (Demartin et al., 1993; Grey et al., 2023a, b), divalent Mn and Mg were allocated at the $M1$ sites, Fe, and Ti at the $M2$ and $M3$ sites and K and O (for H_2O) at the $A1$ and $A2$ sites, and the relative amounts of the pairs of site occupants were refined using Jana2006. The site scattering values and the bond distances for the $M1$ to $M3$

Table 1. Chemical data (wt %) for type paulkerrite.

Constituent	Core of crystals Average of 16			Crystal rims Average of 3		Peacor et al. (1984)	
	Mean	Range	SD	Mean	SD	Standard	
K_2O	5.15	4.36–5.97	0.33	4.96	0.04	4.4	Adularia
MnO	7.42	6.15–9.10	0.69	11.71	0.56	7.1	$MnSiO_3$
MgO	4.51	3.62–5.07	0.39	1.90	0.32	4.6	Spinel
Al_2O_3	1.29	0.47–2.00	0.40	0.18	0.23	1.6	Berlinite
Fe_2O_3	12.66	11.29–14.70	0.89	15.16	1.08	12.2	Hematite
TiO_2	10.85	9.70–11.70	0.61	9.47	0.45	9.8	Rutile
P_2O_5	30.34	26.79–32.68	1.64	29.37	2.78	29.4	Berlinite
F	0.99	0.56–1.50	0.33	1.26	0.18	0.9	Fluorite
H_2O_{calc}	28.8			27.4		30.5	
$-O \equiv F$	−0.42			−0.53		−0.4	
Total	101.59			100.88		100.0	

sites from the refinement were input with chemistry from the EMP analyses to the program OccQP (Wright et al., 2000) to optimise the cation distributions over the different sites. The results showed that the minor Al in paulkerrite preferentially ordered at the $M2$ sites, and so in the next stage of the refinement the Al content from the EMP analyses was evenly distributed at $M2a$ and $M2b$ sites and its occupancy fixed, while the Fe and Ti contents were refined. The site occupancy refinement for the $A1$ and $A2$ sites gave a combined K content of only 0.77 atoms per formula unit (apfu), much lower than the mean EMP value of 1.02 K apfu. With K only at the $A1$ and $A2$ sites, the refined occupancies summed to 1.24 K apfu, well above the mean EMP value. We interpreted these results as indicating some vacancies at the $A1$ and $A2$ sites. Refinements were made using different fixed amounts of vacancies. The best fit to the EMP analysis for K and the lowest R factors in the crystal-structure refinement were obtained for $\sim 18\%$ vacancies at the $A1$ and $A2$ sites. The final refinement in JANA2006 of atom coordinates, site occupancies, and isotropic displacement parameters converged at $R_{obs} = 0.091$ for 2712 reflections with $I > 3\sigma_I$. The high R factor reflects the relatively poor diffracting quality of paulkerrite crystals ($R_{int} = 0.13$) as noted in the study by Peacor et al. (1984). The high R_{obs} for all data results from the large number of very weak reflections. Further details of the data collection and refinement are given in Table 2. Refined atom coordinates, site occupancies, equivalent isotropic displacement parameters, and BVS are given in Table 3. Polyhedral bond lengths are reported in Table 4.

The BVS values are consistent with H_2O at the anion sites O9 to O15. As shown in Table 4 this includes H_2O coordinated to Mn and Mg at the $M1$ sites (O9 to O12), H_2O coordinated to cations at the $M2$ sites (O13), and H_2O coordinated to K at the $A1$ and $A2$ sites (O15). The H_2O at the O14 sites is involved in H-bonding only. The BVS values for the constituents at the X sites are consistent with

a mix of divalent (O^{2-}) and monovalent (F^- and OH^-) at these sites. The relatively low BVS values for many of the oxygen anions, O1 to O8, reflect that they are involved as receptors in multiple H-bonds to the H_2O molecules. Likely H-bonded pairs with O...O less than 3 Å are given in Table 4. The BVS values for constituents at the M sites reflect the ordering of predominantly divalent cations at $M1$, trivalent cations at $M2$, and tetravalent cations at $M3$ sites, consistent with the site occupancy refinements shown in Table 3. The dominance of Mg at $M1$ sites, Fe at $M2$ sites, and Ti at $M3$ sites shown in Table 3 agrees with the formula for paulkerrite given by Peacor et al. (1984):
$KTi(Mg,Mn)_2(Fe^{3+},Al,Ti,Mg)_2(PO_4)_4(OH)_3 \cdot 15H_2O$,
which can be rearranged to
$(H_2O)K(Mg,Mn)_2(Fe^{3+},Al,Ti,Mg)_2Ti(PO_4)_4(OH)_3$
$(H_2O)_{10} \cdot 4H_2O$ to be consistent with more recent formulations (Grey et al., 2023a). Remarkably, the formula of Peacor et al. (1984) was determined without the aid of a crystal structure. The only inconsistency in their formula is the assignment of $[(OH)_3]^{3-}$, whereas the structure determination has the three negative charges provided by two X-site constituents per formula unit $[O(F,OH)]^{3-}$.

The empirical formula in structural form for paulkerrite from the refined site occupancies is as follows:
$^{A1}[K_{0.20}(H_2O)_{0.61}\square_{0.19}]_{\Sigma 1.00} {}^{A2}(K_{0.82}\square_{0.18})_{\Sigma 1.00}$
$^{M1a}(Mg_{0.52}Mn_{0.48})_{\Sigma 1.00} {}^{M1b}(Mg_{0.56}Mn_{0.44})_{\Sigma 1.00}$
$^{M2a}(Fe^{3+}_{0.49}Ti_{0.39}Al_{0.12})_{\Sigma 1.00} {}^{M2b}(Fe^{3+}_{0.49}Ti_{0.39}Al_{0.12})_{\Sigma 1.00}$
$^{M3a}(Ti_{0.47}Fe^{3+}_{0.03})_{\Sigma 0.50} {}^{M3b}(Ti_{0.285}Fe^{3+}_{0.215})_{\Sigma 0.50}(PO_4)_4 X1X2$
$(H_2O)_{10} \cdot 4H_2O$, where $\square$ = vacancy, and the oxygen scattering curve was used for X and H_2O.

The formula shows dominant H_2O at $A1$ and K at $A2$, whereas the pairs of M sites each have the same dominant constituent. The same high degree of K and H_2O ordering between the pairs of A sites but with the same dominant constituent at each of the pairs of M sites also occurs in monoclinic rewitzerite. On this basis the structural

Table 2. Crystal data and structure refinement for paulkerrite.

Ideal formula	$(H_2O)KMg_2(Fe_2^{3+}Ti)(PO_4)_4(OF)(H_2O)_{10} \cdot 4H_2O$
Temperature	100 K
Wavelength	0.7109 Å
Space group	$P2_1/c$ (#14)
Unit-cell dimensions	$a = 10.569(2)$ Å
	$b = 20.590(4)$ Å
	$c = 12.413(2)$ Å
	$\beta = 90.33(3)°$
Volume	2701.2(9) Å^3
Z	4
Absorption correction	Multiscan, $\mu = 1.99$ mm^{-1}
T_{min}/T_{max}	0.41/0.75
Crystal size	$0.025 \times 0.130 \times 0.200$ µm
Theta range for data collection	1.92 to 32.02°
Index ranges	$-15 \le h \le 15, -28 \le k \le 28, -18 \le l \le 18$
Reflections collected	23 111
Independent reflections, R (int)	6830, 0.129
Reflections with $I > 3\sigma_I$	2710
Refinement method	Full-matrix least squares on F
Data, constraints, parameters	6830/24/175
Final R indices [$I > 3\sigma(I)$]	$R_{obs} = 0.091, wR_{obs} = 0.102$
R indices (all data)	$R_{obs} = 0.240, wR_{obs} = 0.116$
Largest diff. peak and hole	1.74 and $-1.92e$ Å^{-3}

formulae can be simplified by combining the $M1a / M1b$, $M2a / M2b$, $M3a / M3b$, and $X1 / X2$, giving for paulkerrite the following formula: $^{A1}[(H_2O)_{0.61}K_{0.20}\square_{0.19}]_{\Sigma1.00}$ $^{A2}(K_{0.82}\square_{0.18})_{\Sigma1.00}$ $^{M1}(Mg_{1.08}Mn_{0.92})_{\Sigma2.00}$ $^{M2}(Fe_{0.98}^{3+}Ti_{0.78}$ $Al_{0.24})_{\Sigma2.00}$ $^{M3}(Ti_{0.75}Fe_{0.25}^{3+})_{\Sigma1.00}$ $(PO_4)_4 X_2(H_2O)_{10}$ $\cdot 4H_2O$. More generally, the formula $A1A2M1_2M2_2M3(PO_4)_4X_2(H_2O)_{10} \cdot 4H_2O$ is given for monoclinic paulkerrite-group members.

2.4 Description of crystal structure

The paulkerrite crystal structure can be described in terms of an alternation of two types of (001) slabs, centred at 1/4, 3/4 and 0, 1/2. These are shown in Fig. 3a and b, respectively. The heteropolyhedral layers at $z = 1/4$ and 3/4 are built from [100] kröhnkite-type chains (Hawthorne, 1985) of four-member rings of corner-connected PO$_4$ tetrahedra and $M2O_4X(H_2O)$ octahedra. Each PO$_4$ tetrahedron also shares a corner with $M1O_2(H_2O)_4$ octahedra along [010] to complete the 2D network of polyhedra. The corner-shared linkages form eight-member rings of alternating octahedra and tetrahedra. The (001) slabs at $z = 0$ and 1/2 comprise isolated $M3O_4X_2$ octahedra together with the A-site constituents (K, H$_2$O) and the zeolitic-type H$_2$O groups at sites O14 and O15. The $M3O_4X_2$ octahedra share their *trans-X* vertices with $M2O_4X(H_2O)$ octahedra in the layers above and below, giving linear trimers that correspond to short segments of the 7 Å chains that are common to many phosphate minerals (Moore, 1970). The $M2$–$M3$–$M2$ trimers are illus-

trated in Fig. 4. A feature of the trimers is short $M2$–X distances, with $M2a$–$X1 = 1.87$ and $M2b$–$X2 = 1.83$ Å, due to displacement of the $M2$-site atoms from the centres of the octahedra towards the bridging X-site anions with the $M3$-centred octahedra. This type of displacement is a common feature of chain structures containing Ti (Bamberger et al., 1990). As shown in Fig. 4, the corner-shared connectivity between the kröhnkite-type chains and the $M3O_4X_2$ octahedra gives rise to 10-member rings, elongated along [100]. The constituents at $A1$ and $A2$ are located in separate rings, centred at 0, y, 0 and 1/2, y, 1/2, respectively.

It is interesting to note that paulkerrite and rewitzerite have different ordering patterns at the A sites. In paulkerrite dominant H$_2$O occurs at $A1$ and dominant K at $A2$, whereas in rewitzerite the ordering is reversed. Potassium at the A sites has a bond to the bridging X-site anion between $M2$- and $M3$-centred octahedra, and the reversal of ordering at the A sites appears to be related to the relative amounts of Ti and (Fe, Al)$^{3+}$ at the $M3$ sites. For paulkerrite, dominant K at $A2$ is coordinated to $X2$, shared with $M3b$, which has a higher Fe^{3+} content than $M3a$ (Table 3), and dominant H$_2$O at $A1$ is coordinated to $X1$, shared with $M3a$, having a higher Ti content than $M3b$. In rewitzerite, where dominant K is at the $A1$ site, it is the $M3a$ site that has a higher (Al + Fe^{3+}) content (0.63 apfu) than the $M3b$ site (0.58 apfu).

Table 3. Refined site occupancies, atom coordinates and equivalent isotropic displacement parameters (Å^2), and bond valence sums (BVS, in valence units) for paulkerrite.

Atom	Occupancy	x	y	z	U_{eq}	BVS
$M1a$	$Mg_{0.521(8)}Mn_{0.479}$	0.49485(10)	0.74723(5)	0.24530(8)	0.0297(3)	2.17
$M1b$	$Mg_{0.562(8)}Mn_{0.438}$	0.99585(10)	−0.24733(5)	−0.24350(8)	0.0297(3)	2.07
$M2a$	$Fe_{0.49(2)}Ti_{0.39}Al_{0.12}$	0.66088(8)	0.50223(4)	0.74653(7)	0.02885(17)	3.19
$M2b$	$Fe_{0.49(2)}Ti_{0.39}Al_{0.12}$	0.16044(8)	−0.00206(4)	−0.74405(7)	0.02885(17)	3.51
$M3a$	$Ti_{0.94(2)}Fe_{0.06}$	0.5	0.5	0.5	0.0295(2)	4.03
$M3b$	$Ti_{0.57(2)}Fe_{0.43}$	0	0	−0.5	0.0295(2)	3.69
$P1a$	1	0.90755(12)	0.59582(7)	0.80049(10)	0.0271(3)	5.05
$P1b$	1	0.40934(12)	−0.09561(7)	−0.80222(10)	0.0267(3)	4.98
$P2a$	1	0.58655(12)	0.59178(7)	0.29474(10)	0.0269(3)	4.98
$P2b$	1	0.08682(12)	−0.09197(7)	−0.29549(10)	0.0267(3)	5.04
$A1$	$O_{0.611(9)}K_{0.20}$	0.7163(3)	0.85261(16)	0.0602(2)	0.0368(4)	0.16
$A2$	$O_{0.005(10)}K_{0.82}$	0.22187(14)	−0.35366(8)	−0.05801(12)	0.0368(4)	0.69
$X1$	1	0.6417(4)	0.50244(15)	0.5963(3)	0.0292(8)	1.47
$X2$	1	0.1412(3)	−0.00324(15)	−0.5976(3)	0.0288(8)	1.53
O1a	1	0.9041(3)	0.66957(19)	0.8043(3)	0.0317(8)	1.72
O1b	1	0.4049(3)	−0.1695(2)	−0.8022(3)	0.0360(9)	1.73
O2a	1	0.0261(3)	0.57226(18)	0.7387(3)	0.0271(7)	1.66
O2b	1	0.5254(3)	−0.07226(18)	−0.7389(3)	0.0286(8)	1.70
O3a	1	0.9094(3)	0.56827(17)	0.9153(3)	0.0283(8)	1.83
O3b	1	0.4129(3)	−0.06899(18)	−0.9174(3)	0.0307(8)	1.88
O4a	1	0.7866(3)	0.57199(18)	0.7427(3)	0.0278(8)	1.80
O4b	1	0.2881(3)	−0.07095(18)	−0.7468(3)	0.0291(8)	1.87
O5a	1	0.5938(3)	0.66489(19)	0.2892(3)	0.0320(8)	1.75
O5b	1	0.0945(3)	−0.16575(19)	−0.2904(3)	0.0317(8)	1.71
O6a	1	0.4670(3)	0.56792(18)	0.2358(3)	0.0282(8)	1.74
O6b	1	0.9661(3)	−0.06820(18)	−0.2366(3)	0.0279(8)	1.70
O7a	1	0.5851(3)	0.56769(18)	0.4115(3)	0.0282(8)	1.89
O7b	1	0.0839(3)	−0.06878(17)	−0.4128(3)	0.0292(8)	1.95
O8a	1	0.7058(3)	0.56443(18)	0.2389(3)	0.0294(8)	1.74
O8b	1	0.2062(3)	−0.06471(18)	−0.2404(3)	0.0289(8)	1.77
O9a	1	0.3477(3)	0.6864(2)	0.1822(3)	0.0363(9)	0.37
O9b	1	0.8468(4)	−0.1875(2)	−0.1831(3)	0.0409(10)	0.34
O10a	1	0.5755(4)	0.74321(19)	0.0830(3)	0.0367(9)	0.34
O10b	1	0.0809(3)	−0.24145(19)	−0.0795(3)	0.0350(9)	0.41
O11a	1	0.6414(3)	0.80693(19)	0.3111(3)	0.0355(9)	0.35
O11b	1	0.1461(4)	−0.3082(2)	−0.3005(3)	0.0396(9)	0.37
O12a	1	0.4026(4)	0.75026(19)	0.4016(3)	0.0370(9)	0.41
O12b	1	0.9073(4)	−0.25260(20)	−0.4069(3)	0.0392(9)	0.29
O13a	1	0.6645(4)	0.50316(16)	0.9168(3)	0.0355(9)	0.36
O13b	1	0.1619(4)	0.00021(16)	−0.9160(3)	0.0347(9)	0.33
O14a	1	0.2585(3)	0.6408(2)	0.4405(3)	0.0396(10)	0
O14b	1	0.7610(3)	−0.14342(19)	−0.4394(3)	0.0365(9)	0
O15a	1	0.5376(4)	0.4082(2)	0.0176(3)	0.0495(11)	0.12
O15b	1	0.0223(4)	0.0950(2)	−0.0112(3)	0.0516(12)	0.02

3 The paulkerrite group

3.1 Approval of the paulkerrite group

Demartin et al. (1997) described paulkerrite (Peacor et al., 1984), mantiennéite (Fransolet, 1984), and benyacarite as members of the paulkerrite group with the general formula $[H_2O,K]_2TiM1_2M2_2(PO_4)_4(O,F)_2 \cdot 14H_2O$,

which can be rearranged to $[H_2O,K]_2M1_2M2_2Ti(PO_4)_4(O,F)_2(H_2O)_{10} \cdot 4H_2O$. A crystal-structure refinement on the related orthorhombic mineral pleysteinite (Grey et al., 2023a) showed dominant Al at the "Ti" site (corresponding to $M3$), requiring the more general formula $A_2M1_2M2_2M3(PO_4)_4X_2(H_2O)_{10} \cdot 4H_2O$, with K and H_2O at A and O, F and OH at X. A fur-

Table 4. Polyhedral bond lengths [Å] for paulkerrite.

$M1a$ −O1b	2.046(4)	$M1b$ −O1a	2.056(4)
−O5a	2.064(4)	−O5b	2.063(4)
−O9a	2.142(4)	−O9b	2.139(4)
−O10a	2.194(4)	−O10b	2.224(4)
−O11a	2.136(4)	−O11b	2.146(4)
−O12a	2.177(4)	−O12b	2.232(4)
avg	2.126	avg	2.143
$M2a$ −X1	1.874(4)	$M2b$ −X2	1.830(4)
−O2b	2.041(4)	−O2a	2.037(4)
−O4a	1.957(4)	−O4b	1.958(4)
−O6a	1.991(4)	−O6b	1.984(4)
−O8b	1.970(4)	−O8a	1.968(4)
−O13a	2.114(4)	−O13b	2.135(4)
avg	1.991	avg	1.985
$M3a$ −X1 ×2	1.912(4)	$M3b$ −X2 ×2	1.929(4)
−O3b ×2	1.982(4)	−O3a ×2	1.996(3)
−O7a ×2	1.992(4)	−O7b ×2	1.988(2)
avg	1.962	avg	1.971
P1a −O1a	1.520(4)	P1b −O1b	1.522(4)
−O2a	1.550(4)	−O2b	1.531(4)
−O3a	1.534(4)	−O3b	1.531(4)
−O4a	1.542(4)	−O4b	1.544(4)
avg	1.536	avg	1.532
P2a −O5a	1.509(4)	P2b −O5b	1.523(2)
−O6a	1.537(4)	−O6b	1.553(3)
−O7a	1.532(4)	−O7b	1.533(3)
−O8a	1.548(4)	−O8b	1.538(3)
avg	1.532	avg	1.536
A1 −X1	3.120(5)	A2 −X2	3.105(4)
−O4a	2.842(5)	−O4b	2.900(4)
−O7a	2.827(5)	−O7b	2.820(4)
−O10a	2.716(5)	−O10b	2.762(4)
−O12b	2.911(5)	−O12a	2.906(4)
−O15b	3.031(5)	−O15a	2.822(5)
avg	2.908	avg	2.886

Possible H-bonded O...O pairs. Distances (less than 3 Å) in parentheses.
O1a...O11a (2.82), O1b...O10a (2.92), O1b...O11b (2.77).
O2a...O11b (2.81), O2a...O15b (2.91), O2b...11a (2.84), O2b...15a (2.86).
O3a...O13a (2.91), O3a...O14b (2.85); O3b...O14a (2.81).
O4a...A1 (2.84), O4b...A2 (2.90), O4b...O11b (2.98).
O5a...O13a (2.76).
O6a...O9a (2.82), O6b...O9b (2.84).
O7a...A1 (2.83), O7b...A2 (2.82).
O8a...O14b (2.81); O8b...O14a (2.79).
O10a...A1 (2.72), O10b...A2 (2.76), O12a...A2 (2.91), O12b...A1 (2.91), O15a...A2 (2.82).
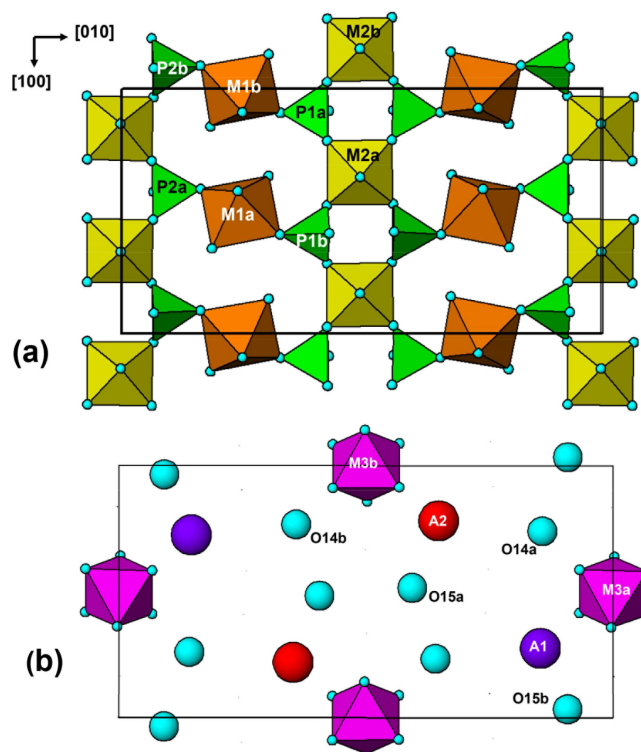
Figure 3. (a) (001) heteropolyhedral layer at $z = 0.25$. **(b)** (001) slab centred at $z = 0$.

ther generalisation was required for the monoclinic mineral rewitzerite (Grey et al., 2023c), which has dominant K at one A site and dominant H_2O at a second A site in $P2_1/c$, consistent with the general formula $A1 A2 M1_2 M2_2 M3 (PO_4)_4 X_2 (H_2O)_{10} \cdot 4H_2O$. The paulkerrite group, with both orthorhombic and monoclinic members, has been approved by the IMA CNMNC, proposal 22-K-bis.

A key feature of the crystal structure of both orthorhombic and monoclinic forms is that M2- and M3-centred octahedra form corner-connected trimers (Fig. 4) corresponding to a short segment of 7 Å chains of octahedra (Moore, 1970), so the octahedra have very similar geometries. For the members for which crystal structures have been refined, there is almost complete mixing of Fe^{3+} and Ti, or Al and Ti, at the similar $M2$ and $M3$ sites. This is illustrated by the empirical formula, in structural form, for the orthorhombic hochleit-nerite (Grey et al., 2023b) below: $^A[(H_2O)_{1.00}K_{1.00}]_{\Sigma 2.00}$ $^{M1}(Mn^{2+}_{1.51}Fe^{2+}_{0.49})_{\Sigma 2.00}$ $^{M2}(Ti^{4+}_{1.08}Fe^{3+}_{0.73}Al_{0.15})_{\Sigma 1.96}$ $^{M3}(Ti^{4+}_{0.54}Fe^{3+}_{0.46})_{\Sigma 1.00}$ $(PO_4)_{4.00}[O_{1.50}F_{0.23}(OH)_{0.27}]_{\Sigma 2.00}(H_2O)_{10} \cdot 4H_2O$.

There is an almost equal distribution of Ti and $(Fe^{3+} + Al)$ at both $M2$ and $M3$ sites, and different end-member formulae can be obtained depending on which site the minor Al is located. The above formula was obtained by application of the least-squares program OccQP (Wright et al., 2000) to
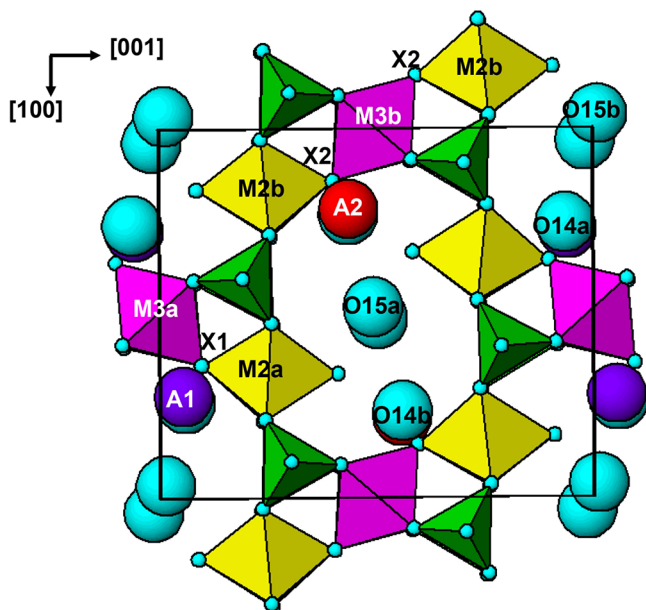
Figure 4. (010) slice through the crystal structure of paulkerrite.

Figure 5. Ternary ($M2_2M3$) composition diagram showing the location of empirical compositions for paulkerrite group members. Blue crosses correspond to Mg dominant at the $M1$ site, whereas red crosses have Mn dominant at $M1$.

optimise the $M1$ to $M3$ site assignments based on the refined site scattering and bond lengths, combined with the chemical analyses. This approach results in the end-member formula $(H_2O)_2Mn_2Ti_3(PO_4)_4O_2(H_2O)_{10} \cdot 4H_2O$ with dominant Ti at both the $M2$ and $M3$ sites. A serious problem with this formula is that it does not contain K (which would give a charge imbalance) even though the empirical formula has equal amounts of K and H_2O at the A site. If the minor Al is constrained to the $M3$ site rather than the $M2$ site, the application of the program OccQP gives dominant Fe^{3+} rather than Ti at the $M3$ site and leads to the alternative end-member formula $[(H_2O)K]Mn_2Ti_2Fe(PO_4)_4O_2(H_2O)_{10} \cdot 4H_2O$, which now has K co-dominant at the A site. The end-member formula ambiguity in paulkerrite-group minerals, due to a high degree of mixing of Ti and (Fe^{3+}, Al) at the $M2$ and $M3$ sites, can be overcome by merging the compositions of the two sites. The unambiguous end-member can then be obtained using the site-total-charge method (Bosi et al., 2019a, b) applied to the empirical formula with Fe^{3+}, Al, and Ti cations considered as disordered over the $M2$ and $M3$ sites. In particular, the site-total-charge method is divided into two steps: one, identifying the dominant end-member charge arrangement from the empirical formula and, two, deriving the dominant end-member formula from this end-member charge arrangement. A list of possible end-member charge arrangements for paulkerrite group minerals with merged $M2$ and $M3$ sites is given in Table 5. A particular advantage of this approach is that the end-member formula can be determined disregarding the cation disorder (i.e. from chemical analyses alone) without the need to obtain bond lengths and site scattering for individual sites from a crystal structure refinement. Such an approach will be very useful in the clas-

sification of paulkerrite-group-containing specimens in museums and private collections.
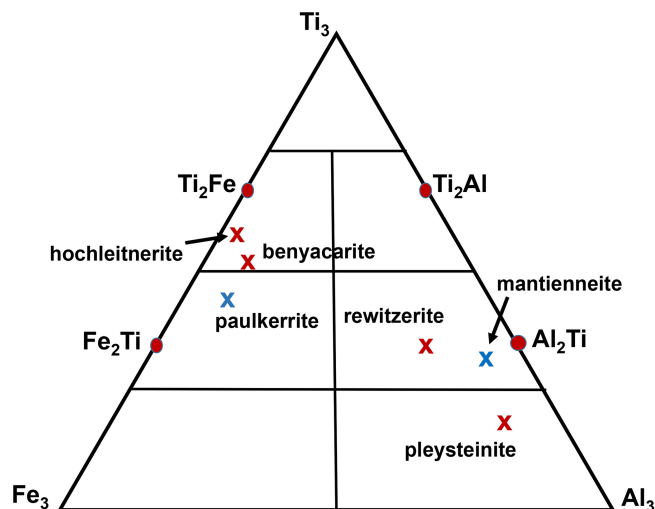
3.2 Application of the merged-site procedure

Merging $M2$ and $M3$ sites in paulkerrite group minerals, the following atomic arrangements are consistent with an end-member composition: (Al_3), (Al_2Ti), (Ti_2Al), (Ti_3), (Fe_3), (Fe_2Ti), (Ti_2Fe).

In accord with the formula $A1A2M1_2(M2_2M3)$ $(PO_4)_4X_2(H_2O)_{10} \cdot 4H_2O$, the possible end-member charge arrangements are given in Table 5. For visualising the different compositions of merged ($M2_2M3$) sites, a ternary diagram should be divided by considering the endmembers Ti_3, Ti_2Al, Al_2Ti, and Al_3 along the Ti–Al edge and Ti_3, Ti_2Fe, Fe_2Ti and Fe_3 along the Ti–Fe edge, as shown in Fig. 5.

Crystal structure refinements for five different paulkerrite-group members are consistent in confirming that the $M1$ site is populated predominantly with the relatively large divalent cations ($2^+ = $ Mn, Mg and Fe). The structural empirical formula is then constructed by assigning 2^+ cations (and minor Fe^{3+} if Mg + Mn < 2 apfu, as the size of $Fe^{3+} >$ Ti > Al) to $M1$ and then assigning remaining Fe plus all Al and Ti to the merged ($M2_2M3$) sites. The site-total-charge method (Bosi et al., 2019a) is then applied to determine the dominant merged-site constituents. This is illustrated below for hochleitnerite with the following empirical formula: $^A[(H_2O)_{1.00}K_{1.00}]_{\Sigma2.00}$ $^{M1}(Mn^{2+}_{1.51}Fe^{2+}_{0.49})_{\Sigma2.00}{}^{M2+M3}(Ti^{4+}_{1.62}Fe^{3+}_{1.19}Al_{0.15})_{\Sigma2.96}$ $(PO_4)_4{}^X[O_{1.50}F_{0.23}(OH)_{0.27}]_{\Sigma2.00}(H_2O)_{10} \cdot 4H_2O$.

End-member contributors are the following:

Table 5. Chemographic exploration (Gagné and Hawthorne, 2016) of end-member charge arrangements for paulkerrite-group minerals with merged ($M2_2M3$) sites.

		Examples
1.	$^A(01^+)^{M1}(2^+)_2^{M2+M3}(3_3^+)(5^+2_4^-)_4{}^X(1^-)_2(H_2O)_{10} \cdot 4H_2O$	pleysteinite (Grey et al., 2023a)
2.	$^A(1_2^+)^{M1}(2^+)_2^{M2+M3}(3_3^+)(5^+2_4^-)_4{}^X(2^-1^-)(H_2O)_{10} \cdot 4H_2O$	$K_2MgFe_3(PO_4)_4(OF)(H_2O)_{10} \cdot 4H_2O$ (hypothetical)
3.	$^A(0_2)^{M1}(2^+)_2^{M2+M3}(3_2^+4^+)(5^+2_4^-)_4{}^X(1^-)_2(H_2O)_{10} \cdot 4H_2O$	mantiennéite (revised formula, this study).
4.	$^A(01^+)^{M1}(2^+)_2^{M2+M3}(3_2^+4^+)(5^+2_4^-)_4{}^X(2^-1^-)_2(H_2O)_{10} \cdot 4H_2O$	rewitzerite, paulkerrite (this study).
5.	$^A(1_2^+)^{M1}(2^+)_2^{M2+M3}(3_2^+4^+)(5^+2_4^-)_4{}^X(2^-)_2(H_2O)_{10} \cdot 4H_2O$	$K_2Mg_2Al_2Ti(PO_4)_4O_2(H_2O)_{10} \cdot 4H_2O$ (hypothetical)
6.	$^A(0_2)^{M1}(2^+)_2^{M2+M3}(4_2^+3^+)(5^+2_4^-)_4{}^X(2^-1^-)_2(H_2O)_{10} \cdot 4H_2O$	benyacarite (revised formula, this study).
7.	$^A(01^+)^{M1}(2^+)_2^{M2+M3}(4_2^+3^+)(5^+2_4^-)_4{}^X(2^-)_2(H_2O)_{10} \cdot 4H_2O$	hochleitnerite (revised formula, this study).
8.	$^A(0_2)^{M1}(2^+)_2^{M2+M3}(4^+)_3(5^+2_4^-)_4{}^X(2^-)_2(H_2O)_{10} \cdot 4H_2O$	$(H_2O)_2Mn_2Ti_3(PO_4)_4O_2(H_2O)_{10} \cdot 4H_2O$ (hypothetical)

Table 6. Comparison of end-member formulae previously reported with the new formulae obtained here using the merged ($M2_2M3$) site approach.

Hochleitnerite (Grey et al., 2023b)	$(H_2O)_2Mn_2Ti_3(PO_4)_4O_2(H_2O)_{10} \cdot 4H_2O$
New formula	$[(H_2O)K]Mn_2(Ti_2Fe)(PO_4)_4O_2(H_2O)_{10} \cdot 4H_2O$
SG, unit cell	$Pbca$, $a = 10.5513(3)$, $b = 20.6855(7)$, $c = 12.4575(4)$ Å
Benyacarite (Demartin et al., 1997)	$KTiMn_2Fe_2(PO_4)_4(OF) \cdot 15H_2O$
New formula	$(H_2O)_2Mn_2(Ti_2Fe)(PO_4)_4(OF)(H_2O)_{10} \cdot 4H_2O$
SG, unit cell	$Pbca$, $a = 10.561(5)$, $b = 20.585(8)$, $c = 12.516(2)$ Å
Pleysteinite (Grey et al., 2023a)	$[K(H_2O)]Mn_2Al_3(PO_4)_4F_2(H_2O)_{10} \cdot 4H_2O$
New formula (unchanged)	$[(H_2O)K]Mn_2Al_3(PO_4)_4F_2(H_2O)_{10} \cdot 4H_2O$
SG, unit cell	$Pbca$, $a = 10.4133(8)$, $b = 20.5242(17)$, $c = 12.2651(13)$ Å
Mantiennéite (Fransolet et al., 1984)	$KMg_2Al_2Ti(PO_4)_4(OH)_3 \cdot 15H_2O$
New formula	$(H_2O)_2Mg_2(Al_2Ti)(PO_4)_4(OH)_2(H_2O)_{10} \cdot 4H_2O$
SG, unit cell	$Pbca$, $a = 10.409(2)$, $b = 20.330(4)$, $c = 12.312(2)$ Å
Rewitzerite (Grey et al., 2023c)	$K(H_2O)Mn_2Al_3(PO_4)_4(OH)_2(H_2O)_{10} \cdot 4H_2O$
New formula	$K(H_2O)Mn_2(Al_2Ti)(PO_4)_4[O(OH)](H_2O)_{10} \cdot 4H_2O$
SG, unit cell	$P2_1/c$, $a = 10.444(2)$, $b = 20.445(2)$, $c = 12.269(1)$ Å, $\beta = 90.17(3)°$
Paulkerrite (Peacor et al., 1984)	$KTiMg_2Fe_2(PO_4)_4(OH)_3 \cdot 15H_2O$
New formula	$(H_2O)KMg_2(Fe_2Ti)(PO_4)_4(OF)(H_2O)_{10} \cdot 4H_2O$
SG, unit cell	$P2_1/c$, $a = 10.569(2)$, $b = 20.590(4)$, $c = 12.413(2)$ Å, $\beta = 90.33(3)°$

Note added in press: the orthorhombic unit cells for hochleitnerite and pleysteinite were obtained from laboratory diffractometer studies on single crystals (SCs). Recent SC studies using a synchrotron microfocus beam confirm that the unit cells for these minerals have a small monoclinic distortion, as occurs in the minerals rewitzerite and paulkerrite. It is likely that all paulkerrrite-group minerals with 1 atom of K per formula unit are monoclinic.

– $(H_2O)_2Mn_2Ti_3(PO_4)_4O_2(H_2O)_{10} \cdot 4H_2O$, 50 % contribution, limited by the $^A(H_2O)$ content;

– $[(H_2O)K]Mn_2(Ti_2Fe)(PO_4)_4O_2(H_2O)_{10} \cdot 4H_2O$, 75 % contribution, limited by the ^XO content.

The second formula is the dominant contributor and thus the representative end-member formula for the analysed mineral. This is illustrated graphically in the ternary diagram shown in Fig. 5, where the empirical composition for the merged ($M2_2M3$) sites for hochleitnerite is plotted and seen to be located in the compositional field for the end-member (Ti_2Fe) rather than that for (Ti_3).

Applying the same approach to the other paulkerrite group members gives the end-member formulae reported in Table 6, where they are compared with the original reported formulae. The empirical compositions for the merged ($M2_2M3$) sites for the six paulkerrite group members are plotted in Fig. 5.

A positive outcome from the merged sites procedure is that the empirical compositions at ($M2_2M3$) now all lie in the correct phase fields for the end-member compositions given in Table 6, when plotted on the ternary composition plot, Fig. 5. This gives confidence to be able to classify new occurrences based on a chemical analysis in conjunction with the ternary plot, without having to obtain a single-crystal refinement. This is an advantage as paulkerrite group minerals often have very poorly diffracting crystals (Peacor et al., 1984; Fransolet et al., 1984).

4　Conclusions

The Ti-bearing secondary phosphate minerals paulkerrite, mantiennéite, benyacarite, pleysteinite, hochleitnerite, and rewitzerite form a mineral group as defined by Mills et al. (2009). The group has been approved by the IMA CN-MNC, revised proposal 22-K-bis. It comprises both orthorhombic members, space group $Pbca$, and monoclinic members (rewitzerite and paulkerrite), space group $P2_1/c$, with unit-cell parameters given in Table 6. The general formulae for the group members are as follows:

– $A_2M1_2M2_2M3(PO_4)_4X_2(H_2O)_{10} \cdot 4H_2O$　for orthorhombic species

– $A1A2M1_2M2_2M3(PO_4)_4X_2(H_2O)_{10} \cdot 4H_2O$ for monoclinic species,

where $A = $ K, H_2O, $\square$ $(= $ vacancy); $M1 = $ Mn^{2+}, Mg, Fe^{2+}, Zn, Ca (rarely Fe^{3+}); $M2$ and $M3 = $ Fe^{3+}, Al, Ti^{4+} (and very rarely Mg); $X = $ O, OH, F. In monoclinic species, K and H_2O show an ordering at the $A1$ and $A2$ sites: in paulkerrite H_2O prevails at $A1$ and K at $A2$, whereas in rewitzerite the ordering is reversed. On the other hand, O, (OH), and F show a disordering over the two non-equivalent $X1$ and $X2$ sites, which were hence merged as X_2 in the general formula. In both monoclinic and orthorhombic species, the two non-equivalent $M2$ and $M3$ sites are structurally very similar, and a high degree of mixing of constituents Fe^{3+}, Al, and Ti occurs at these two sites, introducing considerable ambiguity into the calculation of end-member formulae. To overcome this difficulty, we have used an approach that involves merging the compositions of $M2$ and $M3$ and then applying the site-total-charge method. The resulting end-member formulae are reported in Table 6, and the empirical merged-site compositions are plotted in the ternary diagram shown in Fig. 5. The merged-site approach allows end-member formulae to be obtained directly from the chemical analysis without the need to conduct structure refinements to obtain information on the site populations.

References

Aragao, D., Aishima, J., Cherukuvada, H., Clarken, R., Clift, M., Cowieson, N. P., Ericsson, D. J., Gee, C. L., Macedo, S., Mudie, N., Panjikar, S., Price, J. R., Riboldi-Tunnicliffe, A., Rostan, R., Williamson, R., and Caradoc-Davies, T. T.: MX2: a high-flux undulator microfocus beamline serving both the chemical and macromolecular crystallography communities at the Australian Synchrotron, J. Synch. Radiat., 25, 885–891, 2018.

Bamberger, C. E., Begun, G. M., and MacDougall, C. S.: Raman spectroscopy of potassium titanates: Their synthesis, hydrolytic reactions and thermal stability, Appl. Spectrosc., 44, 31–37, 1990.

Bosi, F., Hatert, F., Halenius, U., Pasero, M., Ritsuro, M., and Mills, S. J.: On the application of the IMA-CNMNC dominant-valency rule to complex mineral compositions, Mineral. Mag., 83, 627–632, 2019a.

Bosi, F., Biagioni, C., and Oberti, R.: On the chemical identification and classification of minerals, Minerals, 9, 12 pp., 2019b.

Demartin, F., Pilati, T., Gay, H. D., and Gramaccioli, C. M.: The crystal structure of a mineral related to paulkerrite, Z. Kristallogr., 208, 57–71, 1993.

Demartin, F., Gay, H. D., Gramaccioli, C. M., and Pilati, T.: Benyacarite, a new titanium-bearing phosphate mineral species from Cerro Blanco, Argentina, Can. Mineral., 35, 707–712, 1997.

Farrugia, L. J.: WinGX suite for small-molecule single-crystal crystallography, J. Appl. Crystallogr., 32, 837–838, 1999.

Fransolet, A.-M., Oustriere, P., Fontan, F., and Pillard, F.: La mantiennéite, une novelle espèce minérale du gisement de vivianite d'Anloua, Cameroun, Bull. Mineral., 107, 737–744, 1984.

Gagné, O. C. and Hawthorne, F. C.: Comprehensive derivation of bond-valence parameters for ion pairs involving oxygen, Acta Crystallogr., B71, 562–578, 2015.

Gagné, O. and Hawthorne, F. C.: Chemographic exploration of the milarite-type structure, Can. Mineral., 54, 1229–1247, 2016.

Grey, I. E., Hochleitner, R., Rewitzer, C., Kampf, A. R., MacRae, C. M., Gable, R. W., Mumme, W. G., Keck, E., and Davidson, C.: Pleysteinite, $[(H_2O)_{0.5}K_{0.5}]_2Mn_2Al_3(PO_4)_4F_2(H_2O)_{10} \cdot 4H_2O$, the Al analogue of benyacarite, from the Hagendorf-Süd pegmatite, Oberpfalz, Bavaria, Germany, Eur. J. Mineral., 35, 189–197, https://doi.org/10.5194/ejm-35-189-2023, 2023a.

Grey, I. E., Keck, E., Kampf, A. R., MacRae, C. M., Gable, R. W., Mumme, W. G., Glenn, A. M., and Davidson, C.: Hochleitnerite, $[K(H_2O)]Mn_2(Ti_2Fe)(PO_4)_4O_2(H_2O)_{10} \cdot 4H_2O$, a new paulkerrite-group mineral, from the Hagendorf-Süd pegmatite, Oberpfalz, Bavaria, Germany, Eur. J. Mineral., 35, 635–643, https://doi.org/10.5194/ejm-35-635-2023, 2023b.

Grey, I. E., Hochleitner, R., Kampf, A. R., Boer, S., MacRae, C. M., Mumme, W. G., and Keck, E.: Rewitzerite, $K(H_2O)Mn_2(Al_2Ti)(PO_4)4[O(OH)](H_2O)10 \cdot 4H_2O$, a new monoclinic paulkerrite-group mineral, from the Hagendorf-Sud pegmatite, Oberpfalz, Bavaria, Germany, Mineral. Mag., 1–29, https://doi.org/10.1180/mgm.2023.55, 2023c.

Hawthorne, F. C.: Towards a structural classification of minerals: The $^{vi}M^{iv}T_2\Phi_n$ mineral, Am. Mineral., 70, 455–473, 1985.

Hawthorne, F. C.: The use of end-member charge-arrangements in defining new mineral species and heterovalent substitutions in complex minerals, Can. Mineral., 40, 699–710, 2002.

Hurlbut, C. S.: A new phosphate, bermanite, occurring with triplite in Arizona, Am. Mineral., 21, 656–661, 1936.

Mills, S. J., Hatert, F., Nickel, E. H., and Ferraris, G.: The standardisation of mineral group hierarchies: application to recent nomenclature proposals, Eur. J. Mineral., 21, 1073–1080, 2009.

Moore, P. B.: Crystal chemistry of the basic iron phosphates, Am. Mineral. 55, 135–169, 1970.

Peacor, D. R., Dunn, P. J., and Simmons, W. B.: Paulkerrite a new titanium phosphate from Arizona, Mineral. Rec., 15, 303–306, 1984.

Petříček, V., Dušek, M., and Palatinus, L.: Crystallographic Computing System JANA2006: General features, Z. Krisallogr., 229, 345–352, 2014.

Sheldrick, G. M.: Crystal structure refinement with SHELXL, Acta Crystallogr., C71, 3–8, 2015.

Wright, S. E., Foley, J. A., and Hughes, J. M.: Optimisation of site occupancies in minerals using quadratic programming, Am. Mineral., 85, 524–531, 2000.